Science Arts & Métiers (SAM)
is an open access repository that collects the work of Arts et Métiers Institute of Technology researchers and makes it freely available over the web where possible.

This is an author-deposited version published in: https://sam.ensam.eu
Handle ID: .http://hdl.handle.net/10985/21303

To cite this version :

Sergei EGOROV, Tatiana TARASOVA, Innokentiy SKORNYAKOV, Lamine HATTALI, Laurent GUILLAUMAT, Svetlana TEREKHINA - In-nozzle impregnation of continuous textile flax fiber/polyamide 6 composite during FFF process - Composites Part A: Applied Science and Manufacturing p.106725 - 2021

Any correspondence concerning this service should be sent to the repository Administrator : scienceouverte@ensam.eu

In-nozzle impregnation of continuous textile flax fiber/polyamide 6 composite during FFF process

S. Terekhina [a,*], S. Egorov [b,c], T. Tarasova [b], I. Skornyakov [a,b], L. Guillaumat [a], M.L. Hattali [d]

[a] Arts et Métiers, Campus Angers - Laboratory LAMPA – 2 Bd du Ronceray, 49035 Angers Cedex 1, France
[b] Moscow State University of Technology "STANKIN", 3-A Vadkovskiy Pereulok, 127055 Moscow, Russia
[c] Institute of Machine Tools and Manufacturing, ETH Zürich, Leonhardstrasse 21, 8092 Zürich, Switzerland
[d] Université Paris-Saclay, CNRS, FAST, 91405 Orsay, France

Keywords:
A: Biocomposite
B: Mechanical properties
E: 3-D Printing
in-nozzle FFF impregnation

A B S T R A C T

A simple and customized method is adapted to print the continuous bleached textile flax yarn/polyamide 6 composites by Fused Filament Fabrication. It is allowed to print successfully composite in one shot thanks to in-situ fiber impregnation inside the print head. Three filling patterns (0°, 90° and ± 45°) strategies relative to the tensile loading were adopted to investigate Young Modulus and tensile strength. The best mechanical properties were obtained for the unidirectional composite, where void content and inter-layer delamination decreased with increasing volume fiber fraction. However, the transversal tensile properties remained at their weakest point. Competitive specific elastic properties compared to those of continuous glass fiber/PA printed composites, given by the literature review, were obtained with the potential to compete the latter in infrastructure, automotive industry, and consumer applications. This is possible if only composite void content is decreased, and its yarn/matrix adhesion is improved.

1. Introduction

Fiber-reinforced composites are constantly expanding and widely used in various industrial sectors such as aerospace, wind energy, and automotive. The reason for this choice is due to their lightness, high specific strength and stiffness, good corrosion resistance, and superior fatigue characteristics [1]. In the field of composite materials, low-cost manufacturing technology has been an important topic of research. A wide variety of composites processing methods, such as Liquid Composite Molding (Liquid Resin Injection, Resin Transfer Molding…) [2], hand lay-up [3], and compression molding [3] have been developed. However, most of these methods have a long processing time and requires a lot of energy. The high cost of processing significantly restricted the application and the use of composite material. Also, synthetic reinforced fiber composite may become a problem for health and the environment. Therefore, the major typical challenges are: (i) to replace the synthetic fibers with renewable ones, (ii) to replace the thermosetting matrix with recycled thermoplastic ones, and (iii) to develop a new process with a more competitive energy efficiency. Nowadays, it is highly desirable to use a new-developed and effective manufacturing technology, like Additive Manufacturing (AM) for composites. AM, also known as 3D printing, is defined as a process of adding materials to fabricate objects from CAD models in successive layers [4,5]. This technology enables the fabrication of complex monolithic structures and geometries, with micrometer resolution without using expensive tools or molds. It is expected to revolutionize the manufacturing of components. While several 3D printing processes are available [6,7], printing using a Fused Deposition Modeling (FDM^{TM}) or Fused Filament Fabrication (FFF) [7-9] is particularly widespread because of its simplicity, relatively high speed, and potential for reinventing the design and low-cost process. However, its main drawback is that the printed parts are low in mechanical properties because of the nature of thermoplastic resins which are too weak compared to metallic and ceramic materials [10,11]. The FFF process is also responsible to the low strength in comparison to the traditional methods, like RTM or LRI. Besides, in the FFF process, generally poor adhesion between filaments and layers exists. Therefore, strengthening the materials or products manufacturing by the FFF process can expand the application of this process into various fields. Various methods have been proposed to increase mechanical properties of 3D-printed materials including the optimization

* Corresponding author.
E-mail addresses: Svetlana.Terekhina@ensam.eu (S. Terekhina), egorov@iwf.mavt.ethz.ch (S. Egorov), t.tarasova@stankin.ru (T. Tarasova), Laurent.Guillaumat@ensam.eu (L. Guillaumat), lamine.hattali@universite-paris-saclay.fr (M.L. Hattali).

https://doi.org/10.1016/j.compositesa.2021.106725

of process parameters [12,13], the addition of fillers [14-16], increasing the strength in the bonding between filaments and layers, and using discontinuous/continuous fibers [14,17-21]. Recently, fiber-reinforcement in FFF has been very popular amongst researchers. Most efforts have focused on the development of filaments with short fibers. Continuous synthetic (carbon, glass, or aramid) fiber-based composites are increasingly being studied due to their high level of mechanical performance compared to the discontinuous ones. Two 3D printing approaches exist: (i) printing with pre-impregnated filaments [22,23] and, (ii) printing with simultaneous impregnation of polymer and fiber in the one cylindrical channel of print head [17,20,24]. MarkForged is the first who developed a 3D printer using a plastic filament impregnated with continuous carbon fibers, by using two separate print heads [25]. The process exhibits a higher potential for structural applications with significantly improved mechanical performance. However, the drawback of the process is that the resin-fiber combination is predetermined; the selection of any other resin or reinforcing fibers for 3D printing is impossible.

Recently, more and more attention has been paid to reinforcing plastics with plant fibers [26-28]. Interest in the latter is associated with economic factors, since they are a renewable resource, very light, and their cost is low compared to all other fibers. For this reason, plant fibers are promising to be used in the manufacturing of polymer-based composite materials (PCM) as reinforcement, which is intended to manufacture a wide variety of products not exposed to a humid environment. PCM with this type of fibers has another important advantage - the possibility of processing and reuse.

Matsuzaki et al. [17] were the first authors to study the feasibility of printing continuous natural jute yarn fibers simultaneously with a PLA matrix. The obtained tensile modulus and strength are 5.11 ± 0.41 GPa and 57.1 ± 5.33 MPa, corresponding to 157% and 134% of those obtained by the neat PLA specimen, respectively. However, jute fibers' properties are moderate because of their low fiber content ($v_f = 6.1\%$) while their high linear density (500 Tex). Thereafter, Le Duigou et al. [21] were the first to print successively continuous natural flax fiber/PLA bio-composites with tensile properties ($E_l = 23.3$ GPa, $\sigma_{Lmax} = 253.7$ MPa corresponding to V_f of 30%), comparable to those obtained by conventional processes (thermo-compression, RTM…). However, the authors [21] used the pre-impregnated 3D printing approach, consisting of performing two separate process steps: (i) impregnation of flax fiber by PLA, and then (ii) printing the pre-impregned filament to obtain composite.

The purpose of this study is to adapt in-nozzle impregnation technique used in the FFF process to the novel continuous flax fiber/polyamide (PA) composites, in which the flax fibers are issued from the textile industry. The use of such composites based on this reinforcement is interesting thanks to their low density (lower than fiberglass) and namely, lower linear density compared to the flax fibers traditionally used in the composite as reinforcement, renewability and recyclability, low-cost and availability at high quality, and large range in industry, but also their potential use in the widespread applications.

Nowadays, to the authors' knowledge, the continuous textile flax fiber/ polyamide (PA) composites obtained by the simultaneous in-nozzle impregnation during the FFF process have never been studied nor reported. This could be also explained by different difficulties of PA matrix printing because of both relative high printing temperature (225 °C for PA6) compared to conventionally used PLA (180 °C), and semi-crystalline state that is one of the causes for warping, distortion, and lack of shape stability [29]. The crystallization during FFF process is believed to drastically decrease molecular mobility and can prevent interlayer diffusion to establish sufficiently strong welds between layers. However, the use of PA-based composites is interesting thanks to their excellent mechanical and chemical properties, highlighting their potential for new industrial applications. In addition, this study follows in the footsteps the previous work carried out on the polyamide materials obtained by the FFF process [29-31].

Table 1
Material properties given by Taulman 3D manufacturer.

Material	PA6 (Nylon 230)
Chemical formula	$[NH-(CH_2)_5-CO]_n$
Melting temperature: T_m, °C	195
Glass transition temperature Tg, °C	68
Tensile modulus when 3D printed, MPa	730
Tensile stress when 3D printed, MPa	34
Coefficient of thermal expansion ($x10^{-6}$ K^{-1})	95
Water absorption (% weight increase, saturated)	8.5–10
Density, g/cm^3	1.14

Table 2
Thermal properties of PA6 (Nylon 230) obtained by DSC before and after the FFF process [29] (T_g – glass transition temperature, T_m – melting temperature and X_c – degree of crystallinity).

Name of Specimen	T_g, °C	X_c, %	T_m, °C
PA6 (Nylon 230) before printing	75 ± 3.7	20 ± 0.7	215 ± 0.8
PA6 (Nylon 230) after printing	73 ± 2.5	20 ± 0.2	214 ± 0.5

In this work, the continuous twisted yarn and polyamide 6 (PA6) filament were fed via two separate channels followed by their mixing in the small heated zone before extruding from a conic flat-head nozzle of 0.6 mm diameter. The advantages of this method regarding to in-nozzle impregnation with two printing separate heads "side by side" are: (i) ensures the mixing of the fiber flax and PA resin in the one heated zone allowing thus, both better fiber distribution and impregnation, and (ii) print composite in one-shot that permitting gain time for the industrial applications.

Therefore, the main ideas of this work is to study preliminary the feasibility of the customized in-nozzle impregnation by the FFF process dedicated for the new considered composites. The influence of some processing parameters such as: layer height, hatch distance, and number of layers on the variation of the fiber volume ratio of the printed unidirectional textile flax/PA6 composite, and, thus, on its mechanical performance will be shown. Additionally, the effect of fiber orientation was studied to assess the transverse tensile properties.

2. Materials and methods

2.1. Materials

Commercially available polyamide 6 (PA6) without chemical additives (Nylon 230 filament, provided by Taulman) was used as the matrix material (Table 1). The selected twisted bleached linen yarn of 39Nm, provided by Safilin (France) and dedicated for the textile industry, was used as continuous reinforcement. Its average diameter of 160 ± 34 μm was determined experimentally by optical observation before printing.

One big challenge with PA6 filaments, similarly to flax fibers, is that they are hygroscopic, which means they readily absorb moisture from their surroundings. It is the moisture that the filaments absorb that produces fumes during printing and affects the quality of the printed specimen. To overcome this problem, the drying of the polymer filament and fiber yarns before printing was carried out at 60 °C in a vacuum oven for 6 h until stabilization in weight loss was achieved. All the specimens (obtained composites, flax yarns and neat printed polymer) were then stored in the dry atmosphere of a desiccator prior to testing.

Based on our previous study [29], the thermal properties of PA6 (Nylon 230) obtained by Differential Scanning Calorimetry (DSC) analysis after the FFF process are given in Table 2. These properties are needed for better understanding the FFF process of newly manufactured composite.

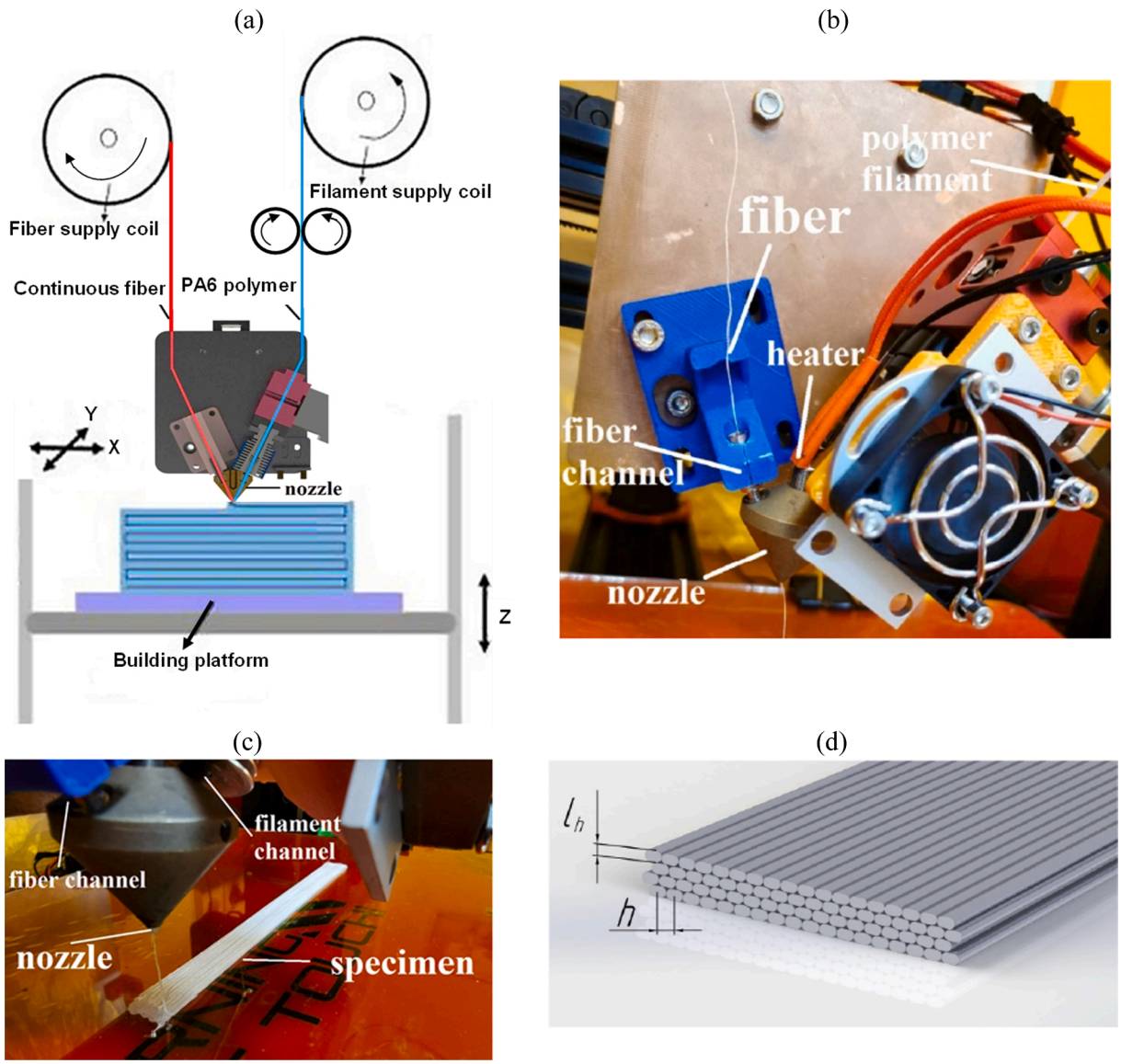

Fig. 1. (a) Schematic of the FFF process of continuous flax/PA6 composite, by using in-nozzle impregnation. (b) Photograph of the modified printer's zone. (c) Magnification view of the 3D printing of a continuous flax/PA6 composite. (d) Schematic of the fixed composite parameters: h – is hatch distance describes the distance to the center of the filament, l_h – layer height.

2.2. 3D printing of continuous fiber composite by in-nozzle impregnation

A TEVO Black Widow 3D printer was used for printing continuous textile flax/PA6 composites. The nozzle of "diamond" shape for 1.75 mm filament has been modified by machining to obtain a custom 0.6 mm conic flat head-nozzle. The use of smaller nozzle diameter than the range of 1.4–1.8 mm [17,21] is necessary to produce a piece with the proper dimensional accuracy and optimum surface finishing. Besides, a flat-head nozzle was used to compact and compress the composite filament to reduce voids in composite.

The modified FFF process of composite consists of supplying a continuous twisted yarn and polyamide 6 (PA6) filament via two separate channels followed by mixing in the small heated zone (linear distance of 2 mm) before extruding from a conic flat-head nozzle (Fig. 1a). Note, the inclined channel in the conic head nozzle for supplying the continuous flax yarn, followed by small size of the heated zone before extruding is very important parameter for successful printing and is necessary to prevent fiber degradation at temperature ≥ 230 °C. Indeed, the fiber stay time in the heated zone is approximately 200 ms. The mixture was then extruded from the nozzle and deposited onto a heated plate. The schematic and two views of this process are presented in Fig. 1a - c.

Table 3
Fixed process parameters along with their nominal values.

Parameter	Value		
Chamber type	closed		
Extruder temperature, °C	225		
Bed temperature, °C	100		
Layer height (l_h), mm	0.3	0.2	0.2
Hatch distance (h), mm	0.55	0.55	0.4
Number of layers (N_l)	4	5	5
Theoretical fiber volume ratio, %	15	18	26
Printing speed, mm/min	600		
Fiber/filament feeding speed, mm/min	600		

A machine-readable g-code obtained by a RepetierHost software has been modified to consider the hatch distance (h) parameter. After conducting many experimental trial runs, the temperature of the nozzle and heating plate was set at 225 °C and 100 °C respectively, and both the fiber/filament feeding and nozzle head speed were 600 mm/min. This

Table 4
Slicing parameters, estimated theoretical and true values of fiber volume ratio V_f of the flax/PA6 composites.

Stacking sequence of composite	$[0]_4$	$[90]_4$	$[\pm45]_4$	$[0]_5$	$[0]_5$
Layer height, mm	0.3	0.3	0.3	0.2	0.2
Hatch distance, mm	0.55	0.55	0.55	0.55	0.4
V_{f_th}, % (equation (1))	15	15	15	18	26
V_{f_true}, % (equation (2))	15 ± 2	15 ± 0.5	14 ± 1	18 ± 1	22 ± 2

speed is enough to ensure a slower cooling which promotes interdiffusion between printed filaments and layers and enhances interlaminar properties of printed samples. The fixed printed composite parameters are schematized in Fig. 1d and given in Table 3.

The estimated fiber volume ratio V_{f_th} of the flax/PA6 composites was determined by the supplied amounts of reinforcing yarns, using the following equation:

$$V_{f_th} = \frac{S_f}{S_c} = \frac{\pi r_f^2 N_f N}{ab} \tag{1}$$

where S_f, S_c – are the section area of flax yarns and composite respectively, r_f – is the radius of flax yarn, N_f – is the number of flax yarns in the ply, N – is the number of plies in the composite, a and b – are the cross-section dimensions of the composite.

Then, the results were verified both using optical examination of the cross-section of the printed composites, and an application of the following Eq. (2). Note, the true fiber volume ratio V_{f_true} is determined by assuming porosity content as zero [32]:

$$V_{f_true} = \frac{1}{\frac{\rho_f}{\rho_m}\left(\frac{1}{\tau_m^f} - 1\right) + 1} \tag{2}$$

where ρ_f, ρ_m – are the densities of fiber (1.44 g/cm^3) and polymeric matrix (1.14 g/cm^3) respectively, given by the manufacturer, τ^f_m – the fiber mass ratio, estimated by:

$$\tau_m^f = \frac{Ntex_f L_f}{m_c} \tag{3}$$

where tex_f – is the linear density (g/1000 m) of flax yarns, L_f - is the length (m) of flax yarns that is used to infill the composite's surface ply, and m_c – is the mass of the composite.

The fiber volume ratio V_f variation was possible thanks to the changes in the layer height (l_h) and the hatch spacing (h) (Fig. 1d). Except for the theoretical value of 26%, the estimated theoretical and true values of V_f of flax/PA6 composites are close enough and were varied between 15 and 22% (Table 4). Samples were printed with a fill density of 100 % with three oriented patterns: (i) 0° (longitudinal), (ii) 90° (transversal), and (iii) ± 45° along the x- axis without any contour (wall layers) (Fig. 2). Supports and brim features were not used.

2.3. Mechanical testing

The tensile properties of the PA6 matrix, flax yarns, and obtained composites were conducted on a universal testing machine (Instron Electropuls E10000) equipped with a 10kN capacity load cell and a strain gauge with a nominal length of 25 mm (Fig. 3). An average sample tests geometry (125 × 10 × 1 mm^3) and the crosshead speed (2 mm/min) were carried out in accordance with ISO 527–4. At least five specimens were tested for each configuration, to evaluate both the Young's modulus and the tensile strength. All tests were performed at room temperature 22 ± 1 °C and at 45 ± 5% Relative Humidity (RH).

2.4. Porosity content

The porosity content was determined according to ASTM D2734-16 [33]:

$$V_p = 1 - \rho_c\left(\frac{\tau_m^f}{\rho_f} + \frac{1 - \tau_m^f}{\rho_m}\right) \tag{4}$$

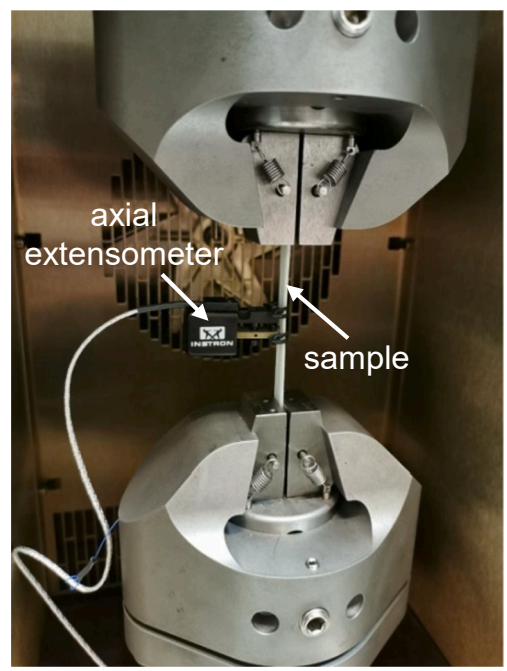

Fig. 3. Electropuls E10000 testing machine.

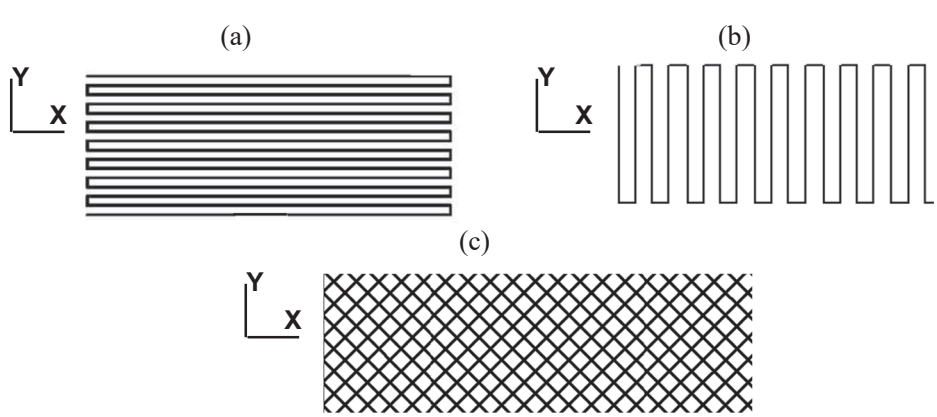

Fig. 2. Schematic views of filling patterns strategy adopted (top view): (a) 0° (longitudinal); (b) 90° (transversal); and (c) ± 45° along the × axis.

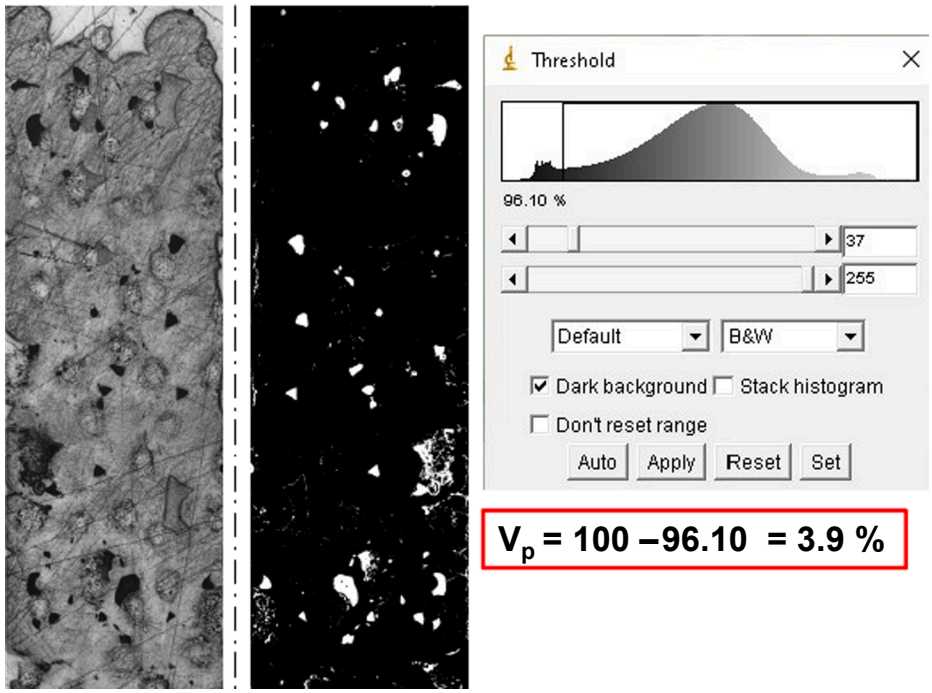

Fig. 4. Analysis of pore size by the Analyze Particles option in ImageJ.

where V_p - is the porosity, ρ_c , ρ_m - are the composite, and matrix densities respectively performed through volumetric and gravimetric test based on Archimedes' principle (Kern ABT-A01), ρ_f - is the fiber density, the value of which is given by the manufacturer, and τ_m^f - is the fiber weight ratio. These voids measurements are verified by image analysis using ImageJ software. A number of optical cross-sections and lengthwise-sections specimens are characterized by image-processing software. The surface area of pores was measured through the "Analyze Particles" option. The first step consists of using thresholding. Raw images are converted to binary images (Fig. 4), in which the object pixels are black, and the pixels representing pores are white. Then, the "Analyze Particles" option is applied (Fig. 4). This command counts and measures objects in thresholded images. It then outlines the object using the wand tool, measures it using the Measure command, fills it to make it invisible, then resumes scanning until it reaches the end of the image or selection. At least five optical images were analyzed for each configuration.

3. Results and discussions

3.1. Microstructure observation

To better understand the microstructure and analyze the pore formation of the continuous textile flax/PA6 composites obtained by the FFF process, the macroscopic views and representative cross-sections of composites were examined using optical microscopy. Fig. 5 (a-c) shows the inter-layer delamination phenomenon at the fibers-matrix deposited filaments interfaces corresponding to $V_f = 15\%$. The delamination was observed whatever fiber orientation applied: $[0]_4$, $[90]_4$, or $[\pm45]_4$. This confirms a poor adhesion of filament inter-layers, especially in contact with fiber yarns. The results of porosity analysis show a high void content ($V_p = [8–14\%]$). Inter-filament area represents the main location of porosity. One of the causes of their formation is the presence of gaps in triangular shapes between filaments formed during the printing.

The warping effect could also be observed with its distortion angle α (Fig. 5 (a-c)). Note, it is very fastidious to print the composite based on PA6 matrix because of its higher relative printing temperature compared to the PLA or ABS polymers (Table.3) and, a semi-crystalline state that is one of the warping causes [29,31]. Fig. 5 (d, f) shows the cross-sections of $[0]_5$ flax/PA6 composites with V_f of 18% and 22% respectively. Our preliminary trials carried out on the relationships between slicing parameters (i.e. layer height (l_h) and hatching distance (h)), and microstructure show that decreasing values parameters results in higher density. A decrease in l_h influences the microstructure and porosity level, whereas a decrease in h allows to increase volume fiber ratio V_f. The combined effect of decreasing these parameters was contributed effectively to eliminate the inter-layer delamination and decrease the void content to 4% in textile flax fiber/PA6 composites. The same trends were observed and discussed for the natural fibers/PLA composites [34,35].

Table 5 presents the average values of pores of the flax/PA6 composites, both measured by Image J and calculated by Eq.4, for different fiber orientations and volume fiber ratio. Fig. 5 (e) confirms that the PA6 resin has poorly impregnated the fiber yarns, by creating decohesion or the interfacial debonding between flax yarn and polymeric matrix. Also, it shows the presence of micro-cracks within the fibrous yarn.

3.2. Tensile mechanical properties

The obtained stress–strain curves for the textile flax twisted yarn, PA6 and textile flax/PA6 composites are shown in Fig. 6a and b, from which the elastic modulus and tensile strength were calculated and are presented in Table 6.

The stress–strain curve of 3D-printed $[0]_4$ oriented flax/PA6 composites shows non-linearity (Fig. 6a). This phenomenon has been already observed in the literature for the conventionally obtained flax reinforced composites [27,28,36]. It could be explained by internal structural changes in the flax yarn and a decrease in the tilt angle of the cellulose fibrils that tend to increase the composite stiffness at the end of tensile testing [37-40] but also attributed to the yielding and viscous behavior of the lignin and amorphous cellulose of the flax fiber because of shear stresses in the cell walls [28]. The tensile modulus and strength of $[0]_4$ oriented flax/PA6 composites are 1.7 (±0.79) GPa and 54 (±4) MPa, respectively, which are 2.4x times and twice higher than those of the neat FFF- printed PA6 polymer.

Unfortunately, the stress and elastic modulus properties of $[90]_4$ and

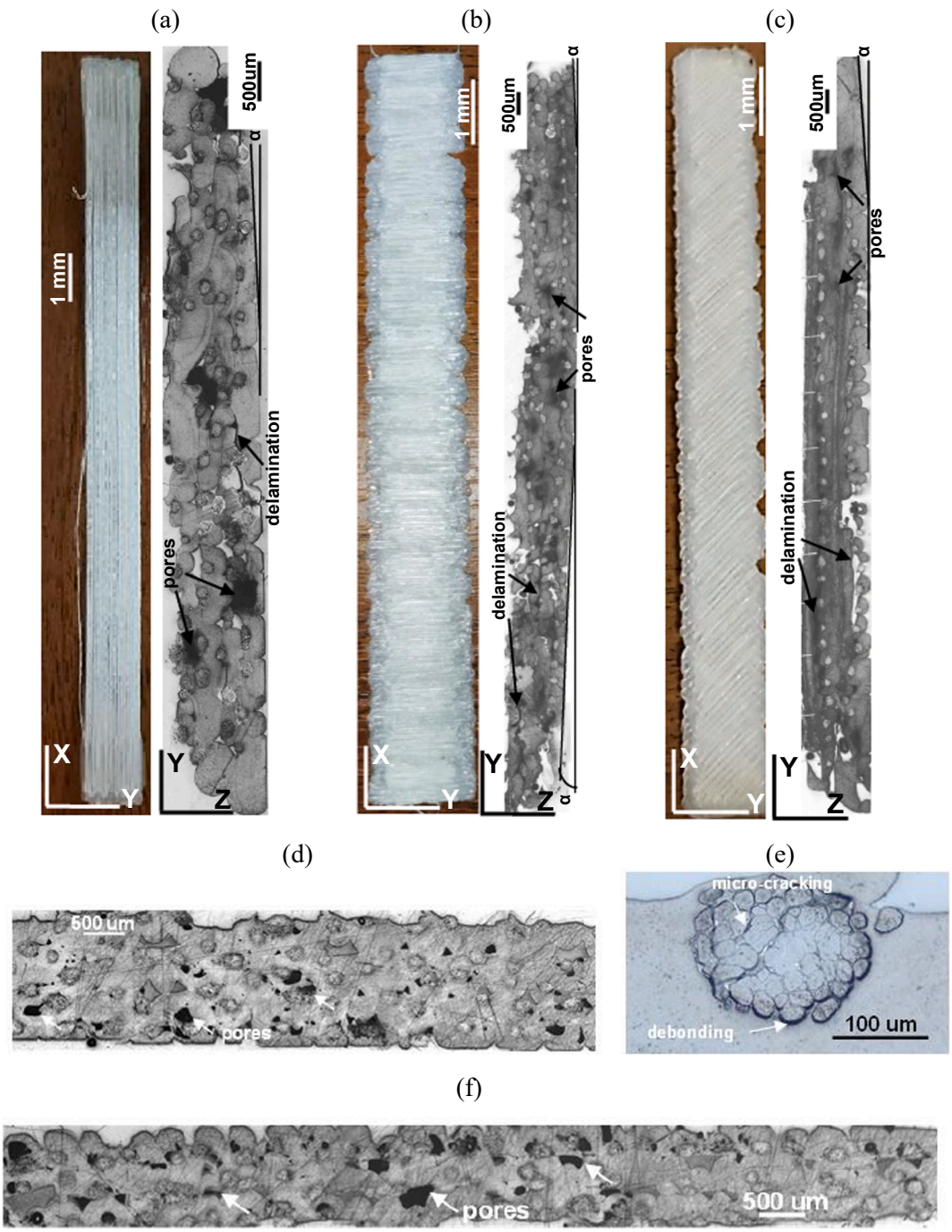

Fig 5. 3D-printed flax/PA6 composites (note : unidirectional fiber composite is aligned with the X-axis, parallel to the direction of the applied load): (a) $[0]_4$, $V_f = 15\%$, α – distortion angle, (b) $[90]_4$,$V_f = 15\%$, (c) $[\pm45]_4$, $V_f = 15\%$; (d) cross-section of $[0]_5$, $V_f = 18\%$, (e) magnification of the cross-section of unidirectional monolayer, (f) cross-section of $[0]_5$, $V_f = 22\%$.

Table 5
Average values of pores of flax/PA6 composites, both measured by Image J and calculated by Eq.4, for different fiber orientation and volume fiber ratio.

Material	$[0]_4$	$[90]_4$	$[\pm45]_4$	$[0]_5$	$[0]_5$
Layer height, mm	0.3	0.3	0.3	0.2	0.2
Hatch distance, mm	0.55	0.55	0.55	0.55	0.4
V_f, %	15 ± 2	15 ± 0.5	14 ± 1	18 ± 1	22 ± 2
Void content V_p, %	14 ± 3	12 ± 1	8 ± 2	4 ± 1	5 ± 0.5

$[\pm45]_4$ oriented flax/PA6 composites are 34x times and more than twice lower for the stresses and 5.6x and 1.75x times for the elastic moduli respectively than those of PA6 polymer printed in longitudinal orientation (Fig. 6, see supplementary Table 6 for a listing of the values). Also, the same low results were observed for their strain-to-failure. The values are decreased to 0.9 ± 0.087 % for $[90]_4$ from the value of 6 ± 0.094 % obtained by the PA6 specimens, because of the lower strain-to-failure characteristics of the flax fibers regarding the capacity of PA6 polymer to strain. The fracture analysis after tensile tests confirms that the flax fibers prevent the free displacement of the PA6 thermoplastic matrix during the axial loading of $[90]_4$ oriented flax/PA6 composite (Fig. 7a). Thus, its value of strain-to-failure is the lowest among all tested

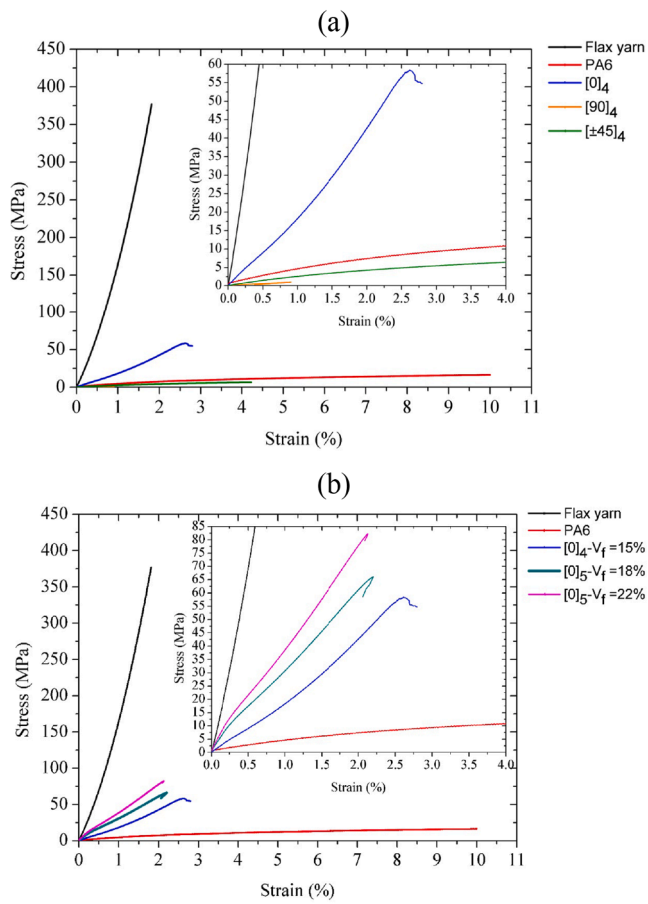

Fig. 6. Stress–strain curves : (a) of flax/PA6 composites ($V_f = 15\%$), depending on fiber orientation that are limited by curves of neat flax twisted yarn and neat PA6 matrix, (b) of unidirectional flax/PA6 composites, depending on fiber volume ratio that are limited by curves of flax twisted yarn and PA6 matrix.

Table 6
Mechanical properties of the tested specimens.

	Young's modulus, GPa	Ultimate tensile strength, MPa
Flax twisted yarns	24 ± 1	377 ± 5
PA6 polymer	0.7 ± 0.2	34 ± 2
$[90]_4$ $V_f = 15\%$	0.125 ± 0.01	1 ± 0.5
$[\pm45]_4$ $V_f = 15\%$	0.4 ± 0.05	14 ± 1
$[0]_4$ $V_f = 15\%$	2.0 ± 0.79	54 ± 4
$[0]_5$ $V_f = 18\%$	4.2 ± 0.6	66 ± 3.5
$[0]_5$ $V_f = 22\%$	5.7 ± 0.5	82 ± 2.5

composite specimens. The decrease in Young modulus and the lack of improvement in the tensile strength for $[90]_4$ and $[\pm45]_4$ orientated flax/PA6 composites could be attributed to the fact that 90° or 45° orientated fibers in composite do not or partially support the axial loading during the tensile tests, and by consequence, all applied stresses are supported only by the PA6 matrix that in our case oriented, in addition, either 90°, or 45° regarding the loading axis. This explains why the tensile properties of $[90]_4$ and $[\pm45]_4$ orientated flax/PA6 composites are lower than those of PA6 specimen printed in a longitudinal direction (Fig. 6a). Therefore, the mechanical properties are improved by 3D printing the PA6 only with continuous unidirectional flax fibers. Note, in all considered fiber orientations of the flax/PA6 composites with 15% of volume fiber ratio, matrix filament cracking and interlayer delamination, followed by fiber pull-out attributed to fracture, are observed in Fig. 7a-c.

As mentioned previously, the adhesion between the fiber yarns and the thermoplastic resin is insufficient. Thereby, the additional treatment surfaces of the fiber is to be indispensable to attain further improvement in mechanical properties. Poor adhesion between thermoplastic resin and reinforcing fibers are common in the manufacturing of thermoplastic-based composites: debonding is usually observed on the fiber yarn /matrix interface [27]. Pores between both polymer and polymer/fiber filaments are also common in FDM-type 3D printing.

The influence of tensile properties of continuous unidirectional textile flax reinforced specimens as a function of volume fiber ratio was also studied (Fig. 6b). Tensile strength and modulus increase with V_f. The tensile modulus and strength of $[0]_5$ flax/PA6 composite with 22% of volume fiber fraction are 5.7 ± 0.5 GPa and 82 ± 2.5 MPa, respectively, which are 3.5x and 1.5x times higher than those of composite with 15% one, and ~ 9x and 2.4x times higher than those of PA6 specimen. The obtained results are summarized in Table 6. The fracture surface after tensile testing of these specimens shows some fiber fractures due to the inter-layer delamination for the composite with 18% of volume fiber ratio, and a neat fiber breakage in the case of $V_f = 22\%$ (Fig. 7 c-e).

Rules of mixture (Eqs. (5) and (6)) were used to estimate both the longitudinal modulus E_L and strength σ_L at longitudinal deformation of 1.8% corresponded to fiber breakage ε_{fL} for the unidirectional fiber reinforced 3D printed composite.

$$E_L = E_f V_f + E_m(1 - V_f), \tag{5}$$

$$\sigma_L = \sigma_f V_f + \sigma_m(1 - V_f), \tag{6}$$

where E_L, and σ_L – the longitudinal modulus and strength of composite, E_f , and σ_f – Young's modulus of strength of fiber, E_m, and σ_m - Young's modulus and strength of matrix at $\varepsilon_{fL} = 1.8\%$, and V_f – volume ratio of fibers. Note that the void contents are not taken into account in the Eqs. (5) and (6).

The theoretical values were then compared with their experimental values (Table 7). The results demonstrate that the mixture law, except for $[0]_4$ composite with $V_f = 15\%$, predicts well an increase of the elastic modulus and strength as fiber reinforcement increases. The error estimation is above 10%. In the case of $[0]_4$ flax/PA6 composite, the experimental longitudinal modulus and its strength are twice and 1.5x times respectively smaller than the theoretical ones. This is explained by poor adhesion between filaments, but also inter-layers, formed initially after the FFF process, which is responsible for delamination.

Furthermore, the elastic properties obtained in this paper can be compared to data compiled from the literature. Fig. 8 compares the specific modulus versus fiber volume ratio data of continuous fiber reinforced PA composites obtained by the FFF from the literature [41-45] and those of this work. Data for conventional flax fiber reinforced PA composite are also shown to serve as a reference. Note, Fig. 8a shows the values of the ratio of longitudinal modulus versus density of composite (E/ρ_c), whereas Fig. 8b – those of longitudinal modulus versus density of fiber (E/ρ_f). It is shown that the obtained $[0]_5$ oriented flax/PA6 composites with V_f of 18% and 22% are very competitive with FFF-printed glass reinforced PA composites. They tend to be the best if the longitudinal modulus E_1 is related to its density of fibers. This ratio also demonstrates its ultra-lightness, relative to other considered synthetic fibers (Fig. 8b). Fig. 9a shows the values of the ratio of longitudinal tensile stress versus density of composite (σ_1/ρ_c), whereas Fig. 9b – those of longitudinal tensile stress versus density of fiber (σ_1/ρ_f). The printed in this work $[0]_5$ oriented flax/PA6 composites with V_f of 22% are close to those obtained conventionally. However, for the same fiber volume ratio, its tensile stress related to its density of composite and fibers respectively is four and three times less than those of glass-reinforced printed composites. This is due to the presence of porosity and poor twisted yarn/matrix adhesion, but also weaker strength resistance of textile flax yarns compared to the glass fibers.

It is necessary to note that the choice of textile flax fiber yarn in the

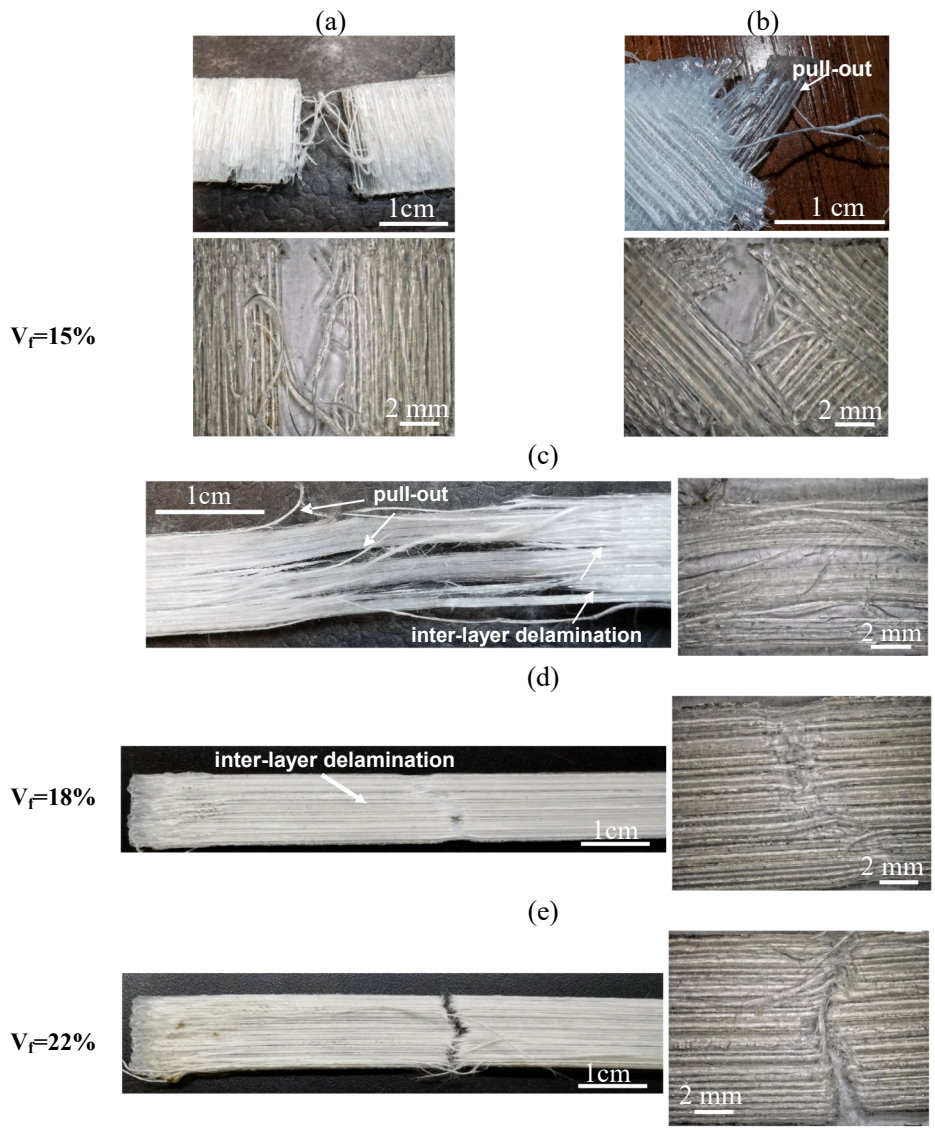

Fig. 7. Fracture of flax/PA6 composites: (a) $[90]_4$, $V_f = 15\%$; (b) $[\pm45]_4$, $V_f = 15\%$, (c) $[0]_4$, $V_f = 15\%$, d) $[0]_5$, $V_f = 18\%$ e) $[0]_5$, $V_f = 22\%$.

Table 7
Comparison of theoretical and experimental data of unidirectional flax/PA6 composites.

	Theoretical elastic modulus, GPa	Experimental elastic modulus, GPa
Flax twisted yarns	–	24 ± 1
PA6 polymer	–	0.7 ± 0.2
$[0]_4$, $V_f = 15\%$	4.0 ± 0.25	2.0 ± 0.79
$[0]_5$, $V_f = 18\%$	4.7 ± 0.12	4.2 ± 0.6
$[0]_5$, $V_f = 22\%$	6.0 ± 0.1	5.7 ± 0.5
	Theoretical tensile strength, MPa	Experimental tensile strength, MPa
Flax twisted yarns	–	377±5
PA6 polymer	–	34±2
$[0]_4$, V_f=15%	63±2	44±4
$[0]_5$, V_f=18%	74±3	64±3.5
$[0]_5$, V_f=22%	90±2	80±2.5

studied flax/PA6 composite was justified by using its lowest linear density (26 Tex) for its better distribution in the composite. This type of fiber was never used before in the FFF process. Therefore, the low linear density of linen yarn and the treatment of flax yarns influence on the obtained mechanical properties that could not be considered competitive with those used actually in 3D printing (non-treated flax fibers with 68 Tex of linear density [21,34]).

Nevertheless, the new-FFF printed unidirectional textile flax/PA6 composites are promising to make use of their better mechanical performance in design and/or non-structural automotive applications. There is yet a possibility to improve their mechanical properties, by attempting 33% of volume fiber ratio during the printing, but also by optimizing the printing parameters that will permit to decrease the void content.

4. Conclusion

In this study, the customized way to produce novel continuous textile flax fiber/PA6 composites manufactured using an inexpensive open-accessible FFF process was presented. The choice of materials is motivated by their potential availability and use in automotive and consumer applications. In addition, on the one side, flax yarns with their cost-

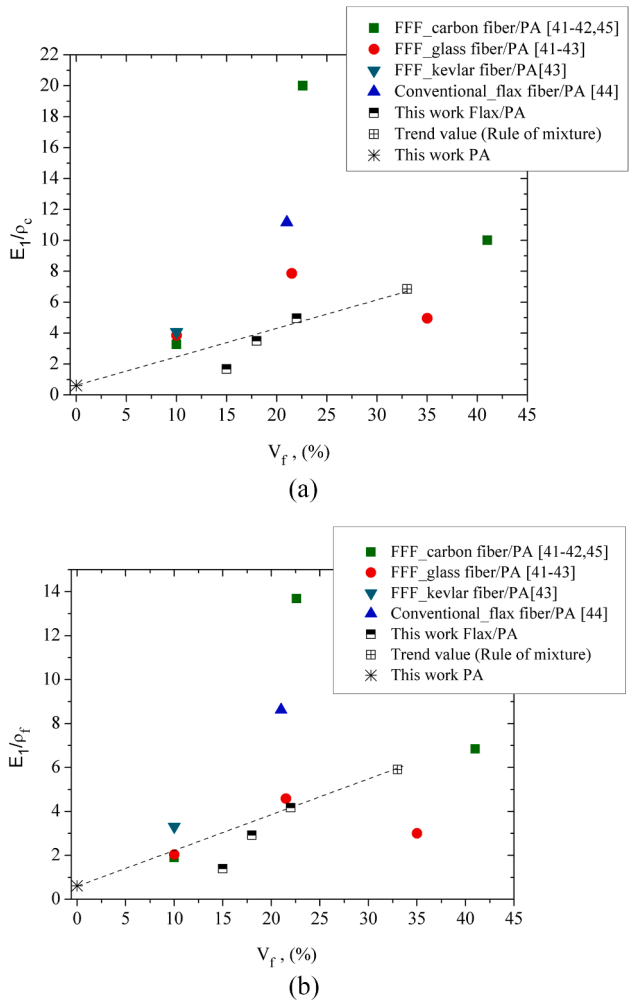

Fig. 8. Comparison of specific tensile modulus versus volume fiber fraction for continuous carbon and glass fiber printed composites [41-45], but also conventional flax/PA composite [44]: (a) E_1/ρ_c versus V_f; (b) E_1/ρ_f versus V_f.

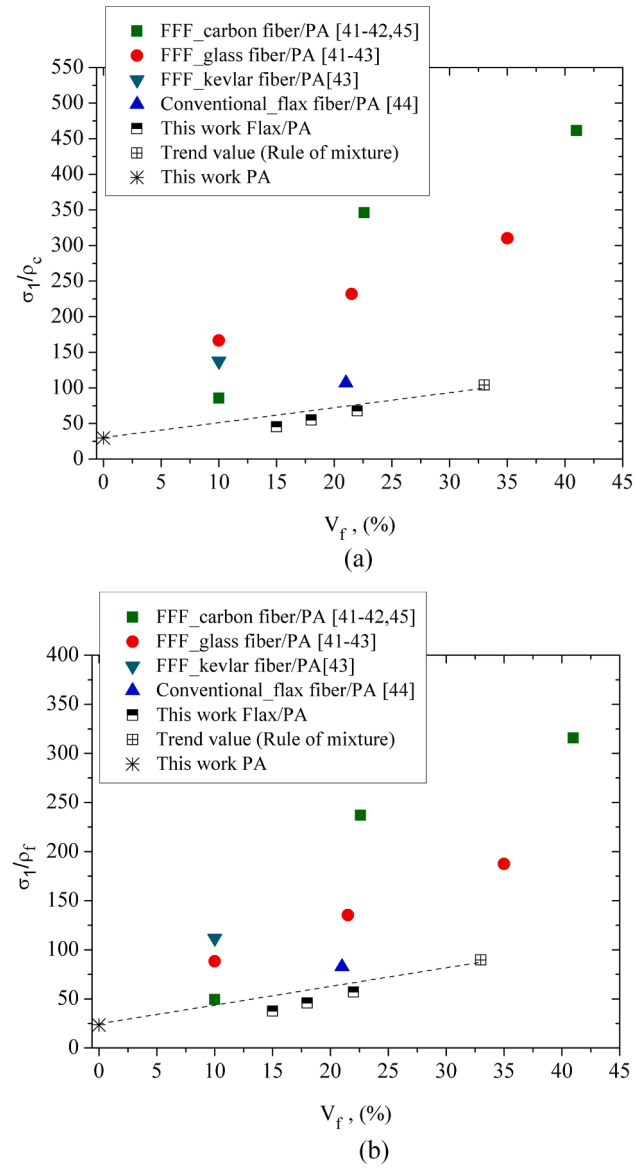

Fig. 9. Comparison of specific tensile stress versus volume fiber fraction for continuous carbon and glass fiber printed composites [41-45], but also conventional flax/PA composite [44]: (a) σ_1/ρ_c versus V_f; (b) σ_1/ρ_f versus V_f.

effective materials and the selected lowest linear weight (26 Tex), usually used in the textile industry, have never been studied before in the FFF process. On the other side, there are no other available continuous natural fiber printed composites based on PA matrix. This is explained by different difficulties to print the latter (its warping, semi-crystalline state…) discussed previously [29,32]. In the modified FFF process, the continuous twisted yarn and polyamide 6 were introduced in two separate channels. The mix of two materials and fiber impregnation process is done into the nozzle in the small heated zone provided for this purpose. The main advantages of the method are: (i) the impregnation process is carried out at the same time as the printing, (ii) the ability to customize the fiber content by varying process parameters or the diameter of head nozzle, the work of which is in the progress, and (iii) prevent the fiber degradation thanks to reducing stay time in the nozzle. The results obtained in this paper were summarized as follows:

- The applied novel strategy led to an important mechanical improvement of composites compared to neat PA6 (9x and 2.4x times for both tensile modulus and strength).
- Selected bleached textile flax yarns with the lowest linear weight (26 Tex) allowed to obtain a reduction in microstructural heterogeneities (for $[0]_5$ with V_f of 18 and 22%).
- The influence of the volume fiber ratio and the fiber orientation on the tensile properties of continuous textile flax fiber/PA6 composites has been studied. It was noticed that tensile properties improved with increasing of volume fiber ratio and decreased drastically with chosen transversal or ± 45° fiber orientation that remained the weakest point of the considered flax reinforced composites. The non-linear tensile behavior was found for the unidirectional textile flax/PA6 composites to be often common for natural fiber unidirectional composites obtained by conventional processes. It has also been highlighted that void content and inter-layer delamination decrease with the rising of V_f in unidirectional textile flax/PA6 composites. In addition, both longitudinal elastic and strength properties were verified by the well-known Rule of Mixture, by demonstrating to be in good agreement with experimental data.
- A major limitation of using flax fibers as reinforcement in composites, and in this case of twisted flax yarns, is the incompatibility which results in poor fiber/matrix interfacial adhesion, by favoring the creation of debonding and pores and thereby, reduces the tensile properties. Therefore, additional physical/chemical modifications are needed to achieve further improvement in mechanical properties.

Note, the purpose of this study is testing the feasibility of the customized FFF process for the new-developed composite material. Future work should be driven to further improve the mechanical properties of printed continuous textile flax/PA6 composite, by increasing its fiber volume ratio (up to 33%), but also the quality of the flax fiber yarn and its filaments. Also, it should be aimed at studying the durability (impact tests, ageing) and long-term behavior (fatigue test) of the obtained composites.

CRediT authorship contribution statement

S. Terekhina: Conceptualization, Funding acquisition, Supervision, Methodology, Writing – original draft. **S. Egorov:** Methodology, Investigation, Data curation, Software. **T. Tarasova:** Funding acquisition, Validation. **I. Skornyakov:** Methodology, Software. **L. Guillaumat:** Writing – review & editing. **M.L. Hattali:** Investigation, Validation, Writing – review & editing.

Declaration of Competing Interest

The authors declare that they have no known competing financial interests or personal relationships that could have appeared to influence the work reported in this paper.

Acknowledgements

The work was carried out with the financial support of the Ministry of Education and Science of the Russian Federation in the framework of state task (project No. 0707-2020-0034). The authors wish to thank Anthony Duval from Safilin SAS for supplying the flax yarns, Benoit Pichereau from Arts et Métiers, Angers Campus, for helpful discussions and technical support. Elena Louicellier, Assessment Services Manager Europe, Cambridge Assessment English, University of Cambridge, post-edited the English style and grammar.

References

[1] Du S. Developing plant fibre composites for structural applications by optimising composite parameters: a critical review. J Mater Sci. 2013;48(18):6083–107.
[2] Long AC. Design and Manufacture of textile Composites. Cambridge: Woodhead Publishing Series in Textiles; 2005.
[3] Flake Campbell Jr. Manufacturing Processes for Advanced Composites. 1st ed. Elsevier, 2003. https://doi.org/10.1016/B978-1-85617-415-2.X5000-X.
[4] ISO / ASTM52900 – 15. Standard Terminology for Additive Manufacturing – General Principles – Terminology.
[5] Gibson I, Rosen D, Stucker B. Additive manufacturing technologies: 3D printing, rapid prototyping, and direct digital manufacturing. Second ed. Springer-Verlag Publ. New York 2015. https://doi.org/10.1007/978-1-4939-2113-3.
[6] Sames WJ, List FA, Pannala S, Dehoff RR, Babu SS. The metallurgy and processing science of metal additive manufacturing. Inter Mater Rev. 2016;61(5):315–60.
[7] Additive manufacturing — General Principles — Overview of process categories and feedstock, ISO/ASTM International Standard. 17296-2:2015(E). 2015.
[8] Wong KV, Hernandez A. A Review of Additive Manufacturing. ISRN Mech Eng. 2012;2012:1–10.
[9] Guo N, Leu MC. Additive manufacturing: technology, applications and research needs. Front of Mech Eng. 2013;8(3):215–43.
[10] Lee CS, Kim SG, Kim HJ, Ahn SH. Measurement of anisotropic compressive strength of rapid prototyping parts. J of Mater Proces Tech. 2007;187-188:627–30.
[11] A. Bagsik, V. Schöppner, Mechanical properties of fused deposition modeling parts manufactured with ultem*9085. In Proceed of 69th Annual Tech Conf of the Soc of Plast Eng (ANTEC'11), 2011; vol. 2, pp. 1294–1298.
[12] Ahn S-H, Montero M, Odell D, Roundy S, Wright PK. Anisotropic material properties of fused deposition modeling ABS. Rapid Prototyp J. 2002;8(4):248–57.
[13] Ghorpade A, Karunakaran KP, Tiwari MK. Selection of optimal part orientation in fused deposition modelling using swarm intelligence. Proc IMechE, Part B: J Eng Manuf. 2007;221(7):1209–19.
[14] Zhong W, Li F, Zhang Z, Song L, Li Z. Short fiber reinforced composites for fused deposition modeling. Mater Sci Eng A. 2001;301(2):125–30.
[15] Ning F, Cong W, Qiu J, Wei J, Wang S. Additive manufacturing of carbon fiber reinforced thermoplastic composites using fused deposition modeling. Compos Part B Eng. 2015;80:369–78.
[16] Wang J, Xie H, Weng Z, Senthil T, Wu L. A novel approach to improve mechanical properties of parts fabricated by fused deposition modeling. Mater Design. 2016; 105:152–9.
[17] Matsuzaki R, Ueda M, Namiki M, Jeong T-K, Asahara H, Horiguchi K, et al. Three-dimensional printing of continuous-fiber composites by in-nozzle impregnation. Sci reports. 2016;6(1). https://doi.org/10.1038/srep23058.
[18] Tekinalp HL, Kunc V, Velez-Garcia GM, Duty CE, Love LJ, Naskar AK, et al. Highly oriented carbon fiber–polymer composites via additive manufacturing. Compos Sci Technol. 2014;105:144–50.
[19] Pidcock GC, in het Panhuis M. & in het Panhuis M. Extrusion Printing of Flexible Electrically Conducting Carbon Nanotube Networks. Advanc Func Mater. 2012;22 (22):4790–800.
[20] Hou Z, Tian X, Zhang J, Zhe Lu, Zheng Z, Li D, et al. Design and 3D printing of continuous fiber reinforced heterogeneous composites. Comp Struct. 2020;237: 111945. https://doi.org/10.1016/j.compstruct.2020.111945.
[21] Le Duigou A, Barbé A, Guillou E, Castro M. 3D printing of continuous flax fibre reinforced biocomposites for structural applications. Mater & Des. 2019;180: 107884. https://doi.org/10.1016/j.matdes.2019.107884.
[22] Der Klift FV, Koga Y, Todoroki A, Ueda M, Hirano Y, Matsuzaki R. 3D printing of continuous carbon fibre reinforced thermo-plastic (CFRTP) tensile test specimens. Open J Compos Mater. 2016;06(01):18–27.
[23] Melenka GW, Cheung BKO, Schofield JS, Dawson MR, Carey JP. Evaluation and prediction of the tensile properties of continuous fiber-reinforced 3D printed structures. Compos Struct. 2016;153:866–75.
[24] Bettini P, Alitta G, Sala G, Di Landro L. Fused deposition technique for continuous fiber reinforced thermoplastic. J Mater Eng Perform. 2017;26(2):843–8.
[25] MarkForged. https://markforged.com, accessed: May 2021.
[26] Pickering KL, Aruan Efendy MG, Le TM. A review of recent developments in natural fibre composites and their mechanical performance. Comp Part A: Appl Sci and Manuf. 2016;83:98–112. https://doi.org/10.1016/j.compositesa.2015.08.038.
[27] Derbali I, Terekhina S, Guillaumat L, Ouagne P. Rapid manufacturing of woven comingled flax/polypropylene composite structures. Int J Mater Form. 2019;12(6): 927–42. https://doi.org/10.1007/s12289-018-01464-1.
[28] Monti A, El Mahi A, Jendli Z, Guillaumat L. Mechanical behaviour and damage mechanisms analysis of a flax-fibre reinforced composite by acoustic emission. Comp Part A: Appl Sci and Manuf. 2016;90:100–10. https://doi.org/10.1016/j.compositesa.2016.07.002.
[29] Terekhina S, Skornyakov I, Egorov S, Guillaumat L, Tarasova T, Hattali ML. The effect of build orientation on both flexural quasi-static and fatigue behaviors of filament deposited PA6 polymer. Int. J. Fatigue. 2020;140:105825. https://doi.org/10.1016/j.ijfatigue.2020.105825.
[30] Terekhina S, Tarasova T, Egorov S, Guillaumat L, Hattali ML. On the difference in material structure and fatigue properties of polyamide specimens produced by fused filament fabrication and selective laser sintering. Int J Adv Manuf Tech. 2020;111(1-2):93–107.
[31] Terekhina S, Tarasova T, Egorov S, Skornyakov I, Guillaumat L, Hattali L. Flexural quasi-static and fatigue behaviours of fused filament deposited PA6 and PA12 polymers. Int J Adv Manuf Tech. 2021 https://link.springer.com/article/10.1007%2Fs00170-021-07223-y.
[32] Gay D. Matériaux composites. 5e edition. Paris: Hermes Science publications; 2005.
[33] ASTM D2734 – 16. Standard Test Methods for Void Content of Reinforced Plastics.
[34] Le Duigou A, Chabaud G, Matsuzaki R, Castro M. Tailoring the mechanical properties of 3D-printed continuous flax/PLA biocomposites by controlling the slicing parameters. Comp Part B: Eng. 2020;203:108474. https://doi.org/10.1016/j.compositesb:2020.108474.
[35] Ayrilmis N, Kariz M, Kwon JH, Kitek Kuzman M. Effect of printing layer thickness on water absorption and mechanical properties of 3D-printed wood/PLA composite materials. Int J Adv Manuf Technol. 2019;102(5-8):2195–200.
[36] Lefeuvre A, Bourmaud A, Morvan C, Baley C. Elementary flax fibre tensile properties:correlation between stress strain behavior and fibre composition. Ind Crops Prod. 2014;52:762–9.
[37] De Rosa IM, Kenny JM, Puglia D, Santulli C, Sarasini F. Tensile behavior of New Zealand flax (Phormium tenax) fibers. J Reinf Plast Compos. 2010;29(23):3450–4.
[38] Baley C, Bourmaud A. Average tensile properties of French elementary flax fibers. Mater. Lett. 2014;122:159–61.
[39] Baley C. Analysis of the flax fibres tensile behaviour and analysis of the tensile stiffness increase. Comp Part A: Appl Sci and Manuf. 2002;33(7):939–48. https://doi.org/10.1016/S1359-835X(02)00040-4.
[40] Du S. Damage in biocomposites: Stiffness evolution of aligned plant fibre composites during monotonic and cyclic fatigue loading. Comp Part A: Appl Sci and Manuf. 2016;83:160–8. https://doi.org/10.1016/j.compositesa.2015.09.008.
[41] Goh GD, Dikshit V, Nagalingam AP, Goh GL, Agarwala S, Sing SL, et al. Characterization of mechanical properties and fracture mode of additively manufactured carbon fiber and glass fiber reinforced thermoplastics. Mater & Des. 2018;137:79–89. https://doi.org/10.1016/j.matdes.2017.10.021.
[42] Chabaud G, Castro M, Denoual C, Le Duigou A. Hygromechanical properties of 3D printed continuous carbon and glass fibre reinforced polyamide composite for outdoor structural applications. Addit Manuf. 2019;26:94–105. https://doi.org/10.1016/j.addma.2019.01.005.
[43] Dickson AN, Barry JN, McDonnell KA, Dowling DP. Fabrication of continuous carbon, glass and Kevlar fibre reinforced polymer composites using additive

manufacturing. Addit Manuf. 2017;16:146–52. https://doi.org/10.1016/j.addma.2017.06.004.
[44] Bourmaud A, Le Duigou A, Gourier C, Baley C. Influence of processing temperature on mechanical performance of unidirectional polyamide 11–flax fibre composites. Indust Crops and Prod. 2016;84:151–65. https://doi.org/10.1016/j.indcrop.2016.02.007.
[45] Liao G, Li Z, Cheng Y, Xu D, Zhu D, Jiang S, et al. Properties of oriented carbon fiber/polyamide 12 composite parts fabricated by fused deposition modeling. Mater & Des. 2018;139:283–92. https://doi.org/10.1016/j.matdes.2017.11.027.